

Article

Experimental Measurement and Theoretical Prediction of Bubble Growth and Convection Heat Transfer Coefficient in Direct Contact Heat Transfer

Jun Yang^{1,2,3,†}, Biao Li^{1,2,3,†}, Hui Sun⁴, Jianxin Xu^{1,2,3,*} and Hua Wang^{1,2,3}

¹ Engineering Research Center of Metallurgical Energy Conservation and Emission Reduction, Ministry of Education, Kunming University of Science and Technology, Kunming 650093, China

² National Joint Engineering Research Center of Energy Saving and Environmental Protection Technology in Metallurgy and Chemical Engineering Industry, Kunming University of Science and Technology, Kunming 650093, China

³ Faculty of Metallurgical and Energy Engineering, Kunming University of Science and Technology, Kunming 650093, China

⁴ Faculty of Science, Kunming University of Science and Technology, Kunming 650093, China

* Correspondence: xinxu@kust.edu.cn; Tel.: +15912469765

† These authors have contributed equally to this work.

Abstract: The measurement of the two-phase contact area is very important to determine the heat transfer coefficient in the process of direct contact heat transfer, but the direct measurement of the two-phase contact area is a difficult problem. The experiments are carried out utilizing a cylindrical Perspex tube of 100 cm in total height and 15 cm inner diameter. The active column height throughout the experiments is taken to be equal to 50 cm. Liquid Therminol[®]66 with four different initial temperatures (50 °C, 60 °C, 70 °C and 80 °C) is used as a continuous phase, while liquid R245fa at a constant temperature of 23 °C is used as a dispersed phase. In this paper, the empirical correlations between bubble growth and local convection heat transfer coefficient are obtained through modeling and measurement, and its correctness is verified by experiments. The results show that the bubble diameter is positively correlated with continuous phase temperature, flow rate ratio, and height, but the local convection heat transfer coefficient is negatively correlated with continuous phase temperature, flow rate ratio, and height. At the same time, it is found that the maximum error between the actual bubble diameter and the theoretical bubble diameter is 7%, and the error between the heat flux calculated by the local convection heat transfer coefficient and the actual heat flux is within 10%. This study provides theoretical guidance for an in-depth understanding of the direct contact heat transfer process and the development of high-efficiency waste heat recovery systems.

Keywords: two-phase flow; bubble dynamics; bubble growth; convection heat transfer coefficient; heat flux



Citation: Yang, J.; Li, B.; Sun, H.; Xu, J.; Wang, H. Experimental Measurement and Theoretical Prediction of Bubble Growth and Convection Heat Transfer Coefficient in Direct Contact Heat Transfer. *Energies* **2023**, *16*, 1069. <https://doi.org/10.3390/en16031069>

Academic Editor: Laura Savoldi

Received: 20 November 2022

Revised: 15 December 2022

Accepted: 19 December 2022

Published: 18 January 2023



Copyright: © 2023 by the authors. Licensee MDPI, Basel, Switzerland. This article is an open access article distributed under the terms and conditions of the Creative Commons Attribution (CC BY) license (<https://creativecommons.org/licenses/by/4.0/>).

1. Introduction

A direct contact heat exchanger (DCHE) is a device that directly contacts cold and hot media for heat exchange [1]. A DCHE has great potential for waste heat recovery owing to its advantage of a low-temperature drive (10–100 °C) [2–5]. To date, many scholars have reported on single bubble dynamics [6–10], bubble group distribution uniformity [11–16], and volumetric heat transfer coefficient (VHTC) measurements [17–28]. However, determining the heat transfer area is also a key scientific issue in explaining the heat transfer process of the DCHE.

Recently, numerous studies have reported bubble dynamics [6–10]. Edel et al. [6] investigated the flow boiling properties of water in a single brass microchannel. According to the experimental results, the growth rate of bubbles enhances with the increase in wall superheat. As the mass flow increases, the bubble growth is inhibited. Cai et al. [7] established

a novel model for the basic heat transfer and mass diffusion mechanism of bubble growth in a homogeneously superheated ethanol–water mixture, showing that the afterward period of bubble growth was primarily affected by mass diffusion. Ghazivini et al. [9] introduced research progress on the bubble growth mechanism and bubble dynamics in boiling. The determination of the empirical correlation formula for the boiling heat transfer coefficient must take into account the bubble dynamics. Mao et al. [10] used a high-speed digital camera to visualize bubble growth characteristics when the supercooled pool was boiling. The experimental results showed that the bubble growth was slow due to the increase in liquid subcooling. Researchers have discussed the heat transfer process from the perspective of a single bubble. However, the study of a single bubble can only be used as a reference and qualitative explanation in engineering practice. This is because it cannot accurately describe the overall state and performance of the heat exchanger. Therefore, it is necessary to explore the relationship between the bubble group and heat transfer performance.

Recently, some studies have also discussed the relationship between bubble group uniformity and the DCHE heat transfer process [11–16]. Xu et al. [11,12] used the L2-Star discrepancy uniform coefficient (UCLD) method to evaluate the bubble mixing time. The linear connection was found between the flow pattern of the bubble group and the heat transfer in a DCHE. Xiao et al. [13–15] studied the layout of bubble groups in a DCHE both theoretically and experimentally. The experiment indicated that there was a good fitting relation among the uniformity of the bubble group distribution and the heat transfer performance. Sun et al. [16] proposed an average distance method to measure the uniformity of bubble group distribution in a DCHE. The bubble groups in the DCHE were treated as random points. The dimensional distribution of the bubble group was determined by calculating the average distance between bubbles. Xu et al. discussed the heat transfer process from the perspective of bubble group uniformity. The experimental results show that there was a good fitting relationship between the uniformity of bubble group distribution and heat transfer performance. The uniformity of the bubble group can describe the trend of the heat transfer performance. However, it cannot accurately characterize the heat transfer performance. Thus, the heat transfer performance can be accurately expressed by calculating the VHTC.

The contact area of the gas–liquid two-phase is difficult to determine owing to the movement and growth of the dispersed phase. The VHTC has been used as an indicator to characterize the direct contact heat transfer performance in many studies [17–28]. Mahood et al. [19,21] used a short column to conduct experimental research on the VHTC of a direct contact condenser. They concluded that the VHTC decreases with increasing time and continuous phase mass flow. Nomura et al. [22–24] studied a DCHE using erythritol as the phase change material. The correlation equation of the VHTC was derived in the process of phase change heat. Barabash et al. [25] used the internal volume of a short vertical tube as the active area for heat and mass transfer. The empirical relationship between heat and mass transfer was obtained. Fu et al. [26–28] studied the area of the liquid–liquid direct contact interface during the heat transfer process of direct contact vaporization. The correlation formula for the VHTC was determined. The VHTC has been used to evaluate heat transfer performance in many studies, but it cannot accurately reflect the heat transfer process. The continuous phase volume is mistaken for the contact volume of the dispersed and continuous phases. However, the dispersed phase was not in contact with all the continuous phases. Therefore, it is necessary to accurately describe the direct contact heat transfer performance by determining the two-phase contact area and obtaining convective heat transfer coefficient.

The goal of this study was to solve the difficulty of measuring the contact area of two phases in the process of direct contact heat transfer. Therefore, the empirical relationship between bubble growth and the local convection heat transfer coefficient was established and verified through models and experiments. In this investigation, the convective heat transfer coefficient accurately characterized the heat transfer performance of the DCHE and described the heat transfer process.

2. Experimental and Research

2.1. Experimental Setup

The experimental setup is shown in Figure 1. The experimental procedure was composed of the Therminol[®]66 circulation and R245fa circulation. The Therminol[®]66 circulation loop consists of a DCHE, gear oil pump (ZCY-1.08, Wenzhou City, Zhejiang Province, China), temperature controller (MDBK-1P-1.1, Jinhua City, Zhejiang Province, China), and an electric heating device (YKX, Yancheng City, Jiangsu Province, China). The overall height of the DCHE was 100 cm, the inner diameter was 15 cm, and the effective height was 50 cm. The R245fa circulation loop consists of a DCHE, condenser, centrifugal pump (ISG25-125, Shanghai City, China), and liquid storage tank. The thermophysical properties of the continuous phase are exhibited in Table 1. The thermophysical characteristics of the dispersed phase are exhibited in Table 2.

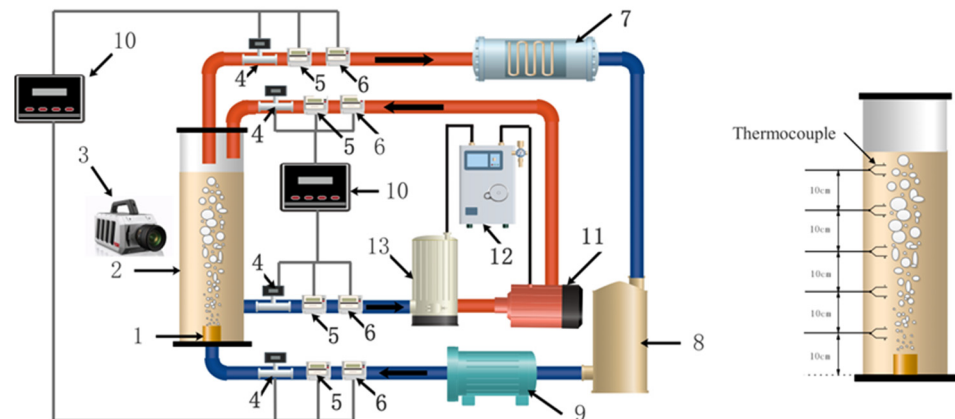


Figure 1. Schematic diagram of the experiment. 1: nozzle; 2: direct contact heat exchanger; 3: high-speed camera (5F01M, Revealer, China); 4: flowmeter; 5: thermometer; 6: pressure gauge; 7: condenser; 8: liquid storage tank; 9: centrifugal pump; 10: instrument display; 11: gear oil pump; 12: control cabinet; 13: electric heater.

Table 1. Thermal properties of the continuous phase.

T_c (K)	ρ_c (kg/m ³)	λ_c (w/(m·k))	$N \times 10^6$ (m ² /s)
323	987.65	0.1163	18.58
333	980.5	0.11575	13.175
343	973	0.1152	7.77
353	969	0.11455	5.98

Table 2. Thermal properties of the dispersed phase.

T_d (K)	$\rho_{d,v}$ (kg/m ³)	$h_{d,L}$ (kJ/kg)	$h_{d,v}$ (kJ/kg)
283	4.8846	212.84	411.79
293	7.1869	225.86	419.12
303	10.169	239.16	426.43
313	14.124	252.27	433.71

2.2. Experimental Process

Therminol[®]66 (continuous phase) in the DCHE was heated by a heater and afterward supplied to the heat exchanger by an oil pump. First, therminol[®]66 was heated to the desired temperature in a heater. Then, Therminol[®]66 was injected from the upper end of the DCHE in a continuous state, and it was ensured that the liquid level reached the required liquid level. There were flowmeters (DN12, Target Type Flowmeter, Huai'an City, Jiangsu Province, China) and a temperature gauge (XMT-101, Nanjing City, Jiangsu Province, China) and pressure gauge (2088, Shanghai City, China), which were used to

gauge the flow, temperature, and pressure of the inlet and outlet of Therminol[®]66. The constant temperature (23 °C) liquid R245fa was sent from the refrigerant storage tank to the DCHE through a centrifugal pump. The liquid mass flow at the inlet of the R245fa was gauged by a flowmeter (DN8, Target Type Flowmeter, Huai'an City, Jiangsu Province, China). In order to gauge the R245fa gas mass flow at the outlet, a flowmeter (DN6, Target Type Flowmeter, Huai'an City, Jiangsu Province, China) was installed. In the DCHE, R245fa and Therminol[®]66 perform direct contact heat exchange. The R245fa underwent a phase change from liquid to gas. Finally, the R245fa steam entered the condenser from the top through the seamless steel pipe. In the condenser, the R245fa steam was condensed and returned to the R245fa storage tank.

Five standard thermocouples were used for the measure temperatures at different locations. These thermocouples were fixed at different heights in the axial direction of the direct contact heat exchanger ($Z_1 = 10$ cm, $Z_2 = 20$ cm, $Z_3 = 30$ cm, $Z_4 = 40$ cm, and $Z_5 = 50$ cm). The thermocouples were connected to a temperature recorder (TS-16A, Shenzhen City, Guangdong Province, China). The measured temperature was displayed on the screen.

The first step in the experiment was to heat the Therminol[®]66. The heater is operated by a temperature controller to ensure that the heat transfer oil reaches the required temperature (50 °C, 60 °C, 70 °C, 80 °C). Then, the Therminol[®]66 was injected into the DCHE. During the experimental cycle, the heat transfer oil inlet temperature was kept constant. The efficacious height of the Therminol[®]66 remained constant in dynamic equilibrium.

When the Therminol[®]66 reached the required temperature, the refrigerant was supplied to start the experiment. The flow rate of the refrigerant was operated using a centrifugal pump. The instrument was calibrated before the start of the operation. During the experiment, the temperature, the pressure, and the flow rate of the entrance and export of the R245fa and Therminol[®]66 were recorded every second. When the R245fa and the Therminol[®]66 started to exchange heat, a high-speed camera was used to capture the heat exchange process of the refrigerant in the heat exchanger. After each set of experiments, the test bench must be cooled to a temperature below 20 °C. Lastly, the refrigerant vapor was condensed into a liquid state by the condenser and then sent back to the liquid storage tank. The experimental working conditions are shown in Table 3.

Table 3. Experimental conditions.

T_c (K)	m_c (kg·s ⁻¹)	m_d (kg·s ⁻¹)
323/333/343/353	0.08	0.08
323/333/343/353	0.08	0.16
323/333/343/353	0.08	0.24
323/333/343/353	0.08	0.32
323/333/343/353	0.08	0.40

2.3. Image Processing and Recognition Process

To observe the growth process of the dispersed phase bubbles in the two phases (R245fa and Therminol[®]66) in the DCHE, a high-speed camera (5F01M, Revealer, China) was used to capture the bubble growth process. The bubble growth process was recorded by a high-speed camera at a speed of 800 frames per second.

Figure 2 shows the image processing procedure and is detailed as follows: (1) original image. Screenshot software (KMPlayer) was used to capture screenshots of the captured videos, taking screenshots every 0.01 s. The original image was preprocessed in grayscale; it is converted into a grayscale image to reduce storage space and improve operational efficiency; (2) binary image. It converts grayscale images to binary images; (3) imopen image. The imopen function should be used not only to eliminate image noise by corroding and expanding the image but also to remove tiny points and smooth the boundaries of larger points without significantly changing the image size. Therefore, the white area

represents the bubble, and the remaining black area represents the liquid phase; (4) imfill image. The imfill function was used to fill the “hole” in the image area.

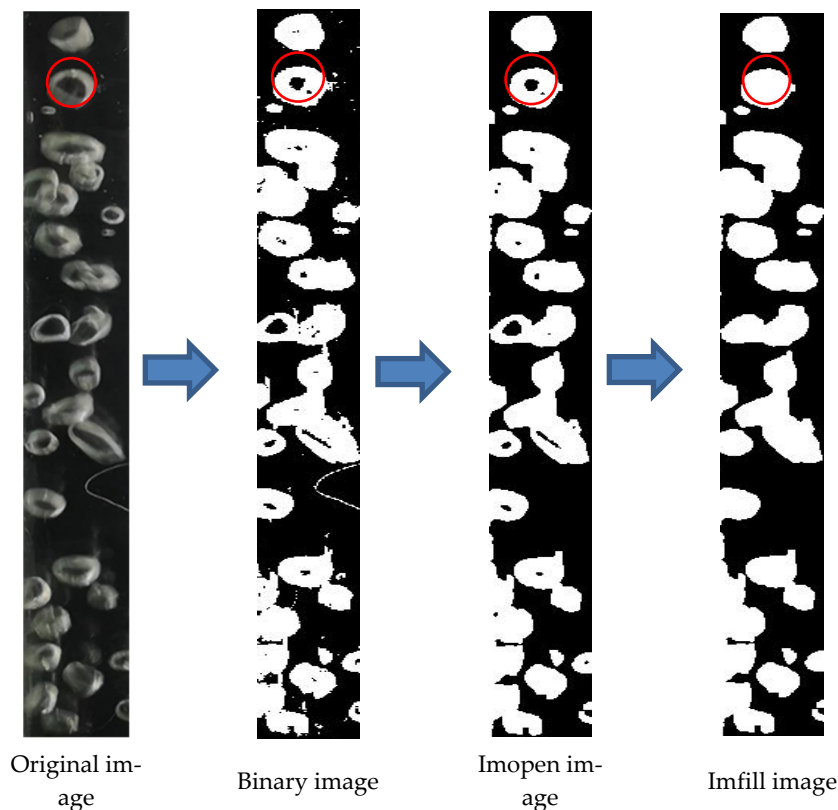


Figure 2. Image processing process.

Finally, the region-props functions in the MATLAB software were used to identify the bubbles, and the centroid coordinate, area, and diameter of the bubbles were obtained.

2.4. Uncertainty Analysis

The uncertainty of the experimental direct measurement data was determined utilizing Equation (1) with 94% certainty interval [29]. The uncertainties of the CHTC and heat transfer quantity were calculated using the uncertainty formula [30]. In this research, the maximum uncertainty of the flowmeter was 0.8%, and the measuring scope of was 50–400 kg/h. The measuring scope of the thermocouple is 0–200 °C. The temperature transducers were connected to a data logger, and the reference zero point was aligned. The measurement and recording precision of the temperature transducers were assessed as ± 1.2 °C and ± 0.6 °C, respectively. Thus, the indeterminacy of temperature measuring was ± 1.34 °C. The measuring precision of Therminol[®]66 fluid level and evaporator diameter were both ± 0.02 m. Consequently, the uncertainty of the liquid level volume was 4.6%.

$$X_r = \sqrt{P_K^2 + B_K^2} \quad (1)$$

where P_K represents the precision stint of the apparatus, and B_K was the error stint.

3. Empirical Correlations

3.1. Bubble Diameter Correlation

The two-phase contact area was determined by calculating the bubble diameter in the DCHE. To simplify the calculation of the bubble diameter, it was necessary to make assumptions regarding the dispersed phase bubbles in the DCHE.

- (1) The bubble was regarded as rigid, and only the volume changes without deformation during the ascending process. The equivalent ball diameter was considered to be the bubble diameter.
- (2) The bubbles were considered not to merge or break during the ascending process.
- (3) The dispersed phase vapor was not retained in the continuous phase.

Based on the above assumptions, Mori et al. [31] calculated the bubble diameter (D_M) using heat balance.

$$\pi D_M^2 h \Delta T dt \approx \rho_{dv} h_{fg} \pi D_M^2 dD_M \quad (2)$$

where D_M , h , ΔT , ρ_{dv} , and h_{fg} represent the theoretical bubble diameter, instantaneous convection heat transfer coefficient of the surface area of the spherical two-phase bubble, temperature difference between the R245fa and Therminol®66, vapor phase density of the dispersed phase, and latent heat of condensation, respectively.

The calculation formula of ΔT was:

$$\Delta T = \Delta T_{min} + (\Delta T_{max} - \Delta T_{min}) \left(\frac{Z}{H} \right) \quad (3)$$

where ΔT_{min} , ΔT_{max} , H , and Z represent the minimum temperature difference between the continuous and dispersed phases, maximum temperature difference between the continuous and dispersed phases, continuous phase liquid level, and position of the bubble, respectively.

The calculation formulas of ΔT_{min} and ΔT_{max} were as follows:

$$\Delta T_{max} = \max\{(T_{c,in} - T_{d,out}), (T_{c,out} - T_{d,in})\} \quad (4)$$

$$\Delta T_{min} = \min\{(T_{c,in} - T_{d,out}), (T_{c,out} - T_{d,in})\} \quad (5)$$

where $T_{c,in}$, $T_{c,out}$, $T_{d,in}$, and $T_{d,out}$ represent the inlet temperature of the continuous phase, outlet temperature of the continuous phase, inlet temperature of the dispersed phase, and outlet temperature of the dispersed phase, respectively.

The formula of Nusselt number proposed by Moalem-Maroon [32] was as follows,

$$Nu = C_1 Pe^{0.5} = \frac{h D_M}{\lambda_c} \quad (6)$$

where Nu , Pe , and λ_c represent the Nusselt number, Peclet number, and thermal conductivity of the continuous phase, respectively. According to Shimizu et al. [33], the calculation formula for C_1 was as follows:

$$C_1 = \frac{\int_0^{t_v} D_M Nu \Delta T dt}{\int_0^{t_v} D_M Pe^{0.5} \Delta T dt} \quad (7)$$

where t_v represents the time required for complete evaporation. According to the experimental conditions, C_1 was $\frac{2}{\pi^{0.5}}$.

In previous studies, Vikas Chaurasiya et al. [34] found that when Ste (Stefan number) was fixed, the melting process becomes fast with increasing the value of Pe , i.e., Pe accelerated the transition process and changed the thermal conductivity. The Peclet number can be expressed as follows:

$$Pe = \frac{U_r D_M}{\epsilon_d} \quad (8)$$

where U_r , and ϵ_d represent the relative speed of the R245fa and Therminol®66, and the thermal diffusivity of the R245fa, respectively. By substituting Equations (7) and (8) into Equation (6), the expression for h can be obtained as follows:

$$h = \frac{2}{\pi^{0.5}} \frac{U_r^{0.5} \lambda_c}{D_M^{0.5} \epsilon_d^{0.5}} \quad (9)$$

The relationship between bubble rise height and bubble velocity was calculated as follows:

$$dz = Udt \quad (10)$$

where U represents the rising speed of the bubble. Substituting Equations (9) and (10) into Equation (2), and simplifying it was as follows:

$$D_M^{0.5} dD_M = \frac{2}{\pi^{0.5}} \left(\frac{U_r}{\epsilon_d} \right)^{0.5} \left(\frac{\lambda_c}{\rho_{dv} h_{fg}} \right) U^{-1} \Delta T dZ \quad (11)$$

Equation (11) was integrated. $Z = 0$ and $D_M = D_0$ was substituted into Equation (11) as follows:

$$\frac{2}{3} D_M^{1.5} = \frac{2}{\pi^{0.5}} \left(\frac{U_r}{\epsilon_d} \right)^{0.5} \left(\frac{\lambda_c}{\rho_{dv} h_{fg}} \right) U^{-1} \Delta T Z + \frac{2}{3} D_0^{1.5} \quad (12)$$

To simplify Equation (12), the ratio w was introduced as follows:

$$w = \frac{U_r}{U} \quad (13)$$

where w represents the ratio of relative velocity to bubble velocity. Equations (3) and (13) were substituted into Equation (12), as follows:

$$D_M = \left\{ D_0^{1.5} + 3 \left(\frac{1}{\pi \epsilon_d U_r} \right)^{0.5} \times \left(\frac{\lambda_c}{\rho_{dv} h_{fg}} \right) \times w \times \left[\Delta T_{min} \times Z + (\Delta T_{max} - \Delta T_{min}) \left(\frac{Z^2}{H} \right) \right] \right\}^{\frac{2}{3}} \quad (14)$$

where D_0 represents the nozzle diameter. Prasser et al. [35] found that the growth of bubbles with different pipe diameters was significantly different. In addition, Vafaei et al. [36] found that the diameter of the spray nozzle has a forceful effect to bubble growth. In the DCHE heat exchange process, it was indispensable to discuss the effect of the diameter of the DCHE and nozzle diameter on bubble growth. Therefore, to obtain a more accurate relationship, the constant $C_2 = \left(\frac{D_0}{d} \right)^{C_3}$ was introduced to modify Equation (14). When C_3 was -0.125 , its correlation was as high as 0.998235. Thus, when C_2 was $\left(\frac{D_0}{d} \right)^{-0.125}$, the relationship between bubble growth was as follows:

$$D_M = \left(\frac{D_0}{d} \right)^{-0.125} \left\{ D_0^{1.5} + 3 \left(\frac{1}{\pi \epsilon_d U_r} \right)^{0.5} \times \left(\frac{\lambda_c}{\rho_{dv} h_{fg}} \right) \times w \times \left[\Delta T_{min} Z + (\Delta T_{max} - \Delta T_{min}) \left(\frac{Z^2}{H} \right) \right] \right\}^{\frac{2}{3}} \quad (15)$$

where d denotes the diameter of the heat exchanger. The heat exchange area can be determined by the bubble diameter.

3.2. Local Convection Heat Transfer Coefficient Correlation

It was difficult to determine the two-phase contact area in the DCHE. Therefore, an empirical correlation of the local convection heat transfer coefficient correlation between R245fa and Therminol[®]66 can be derived.

Mori et al. [31] considered that the local convection heat transfer coefficient can be calculated by Equation (16).

$$h_Z = n\pi D_M^2 h \quad (16)$$

where h_Z and n represent the local convection heat transfer coefficient and number of local two-phase bubbles, respectively. D_M and h have already been derived in 3.1. By substituting Equations (9) and (15) into Equation (16), the expression for h_Z can be obtained as follows:

$$h_Z = 2n\lambda_c \left(\frac{\pi U_r}{\epsilon_d} \right)^{0.5} D_M^{\frac{3}{2}} \quad (17)$$

In order to obtain an accurate correlation of the local CHTC, the effects of the temperature of the R245fa and Therminol[®]66 were considered. Therefore, the constant $C_3 = \left(\frac{T_c}{T_d}\right)^{C_4}$ was introduced to modify Equation (17). When C_4 was 4, its correlation was as high as 0.997612. Thus, when C_3 was $\left(\frac{T_c}{T_d}\right)^4$, the empirical correlation of local convection heat transfer coefficient was as follows:

$$h_Z = 2n\lambda_c \left(\frac{\pi U_r}{\epsilon_d}\right)^{0.5} D_M^{\frac{3}{2}} \left(\frac{T_c}{T_d}\right)^4 \quad (18)$$

3.3. Calculation of Q_T and Q_Z

During direct contact heat transfer, Baqir et al. [37] believed that latent heat dominated phase transformation, so the actual heat flux (Q_T) can be calculated as the following formula:

$$Q_T = m_d(H_{d,out} - H_{d,in}) \quad (19)$$

where m_d , $H_{d,out}$, and $H_{d,in}$ represent the mass flow rate of the R245fa, outlet enthalpy of the dispersed phase, and inlet enthalpy of the dispersed phase, respectively.

According to Equation (18), the local convection heat transfer coefficient was obtained. The theoretical heat transfer quantity (Q_Z) was calculated as follows:

$$Q_Z = h_Z A \Delta T_{tm} \quad (20)$$

where A and ΔT_{tm} represent the heat exchange area and logarithmic average temperature difference between the R245fa and Therminol[®]66, respectively.

The calculation of A was as follows:

$$A = \sum_{i=1}^n 4\pi r_i^2 = \sum_{i=1}^n \pi D_{i,M}^2 \quad (21)$$

where i , r_i , and $D_{i,M}$ represent the variable, theoretical radius of the i -th bubble, and theoretical diameter of the i -th bubble, respectively.

The calculation of ΔT_{tm} was as follows:

$$\Delta T_{tm} = \frac{\Delta T_{max} - \Delta T_{min}}{\ln\left(\frac{\Delta T_{max}}{\Delta T_{min}}\right)} \quad (22)$$

4. Results and Discussion

4.1. Bubble Diameter

The growth process of dispersed phase bubbles was observed using a high-speed camera. Digital image processing was used to process bubbles to obtain their actual diameter (D_T). However, the actual diameter of the bubble can only be obtained through complex image processing. Therefore, the bubble's thermal balance formula was used to derive the bubble's theoretical diameter (D_M) growth formula, thereby simplifying the image processing.

The relationship between bubble diameter and height is shown in Figures 3 and 4. Figures 3 and 4 show that, with the same temperature, the bubble diameter increased with an increase in height. Therefore, the bubble diameter increased with height [38]. Another reason was that an increase in height caused a decrease in pressure. The decrease in pressure will lead to an increase in buoyancy, decrease in basset force, and liquid resistance. Therefore, decrease in pressure leads to the enlargement of the bubble diameter.

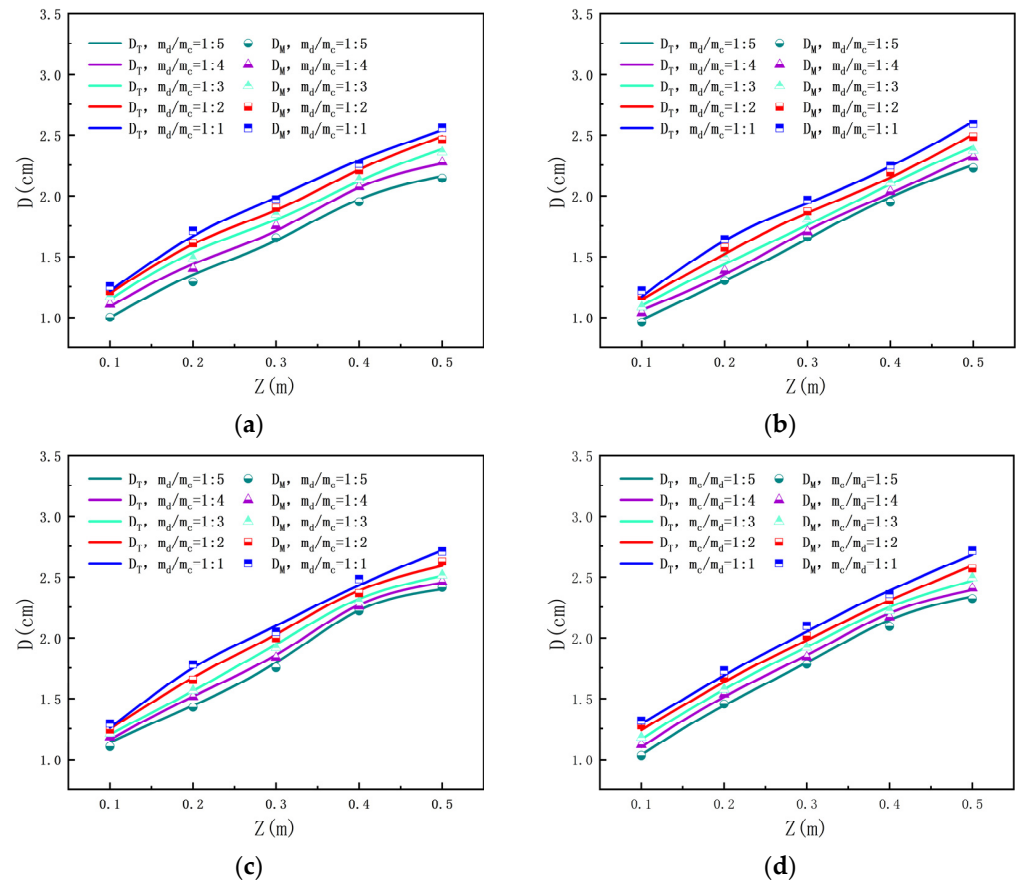


Figure 3. The relationship between bubble diameter and height (Z) at different temperatures. (a): $T_c = 50^\circ\text{C}$. (b): $T_c = 60^\circ\text{C}$. (c): $T_c = 70^\circ\text{C}$. (d): $T_c = 80^\circ\text{C}$.

Figure 3 also shows the relationship between the bubble diameter and flow rate ratio. Figure 3 shows the positive correlation between bubble diameter and flow ratio at the same temperature. The bubble diameter was largest when the flow rate ratio was 1:1. This was because the flow rate of the R245fa was constant, and an increase in the flow ratio indicated a decrease in the flow rate of the Therminol[®]66. Consequently, the viscous shear force caused by the Therminol[®]66 decreased. Therefore, the time for the bubble to overcome the Young–Laplace force became longer, and the bubbles continued to grow.

Equation (15) shows that the thermophysical properties of the Therminol[®]66 have a significant effect on bubble growth. Figure 4 shows the relationship between the bubble diameter and Therminol[®]66 temperature. When the temperature of the Therminol[®]66 increased, the bubble diameter also increased. Figure 4a shows that when the flow ratio was 1:1, the continuous phase temperature was 80°C , and the bubble diameter was the largest. This was because the influence of temperature on bubble size was attributed to the change in physical properties. At the same time, the increase in temperature led to a decrease in liquid density, viscosity, surface tension, and gas density and an increase in saturated vapor pressure. The saturated vapor pressure in this experiment cannot be ignored, resulting in the bubble diameter increasing with temperature [39].

Figures 3 and 4 show the relationship between D_T and D_M under different working conditions. Figures 3 and 4 show the trend of the bubble diameter growth correlation close to that of the experimental data. This was because the correlation considers that the diameter of the heat exchanger and nozzle affected bubble growth. As shown in Figures 3 and 4, the D_M was evenly distributed around D_T . When the continuous phase temperature was 50°C , the flow rate ratio was 1:1, and the height was 0.2 m, the error between D_M and D_T was 7%. This was presumably because the growth of bubbles in the Therminol[®]66 was imperfect. The pressure of the R245fa affects the change in viscous shear force and further

affects the growth of bubbles [40]. Further development and modification of the proposed correlation are required in future studies to investigate the effects of multiple parameters.

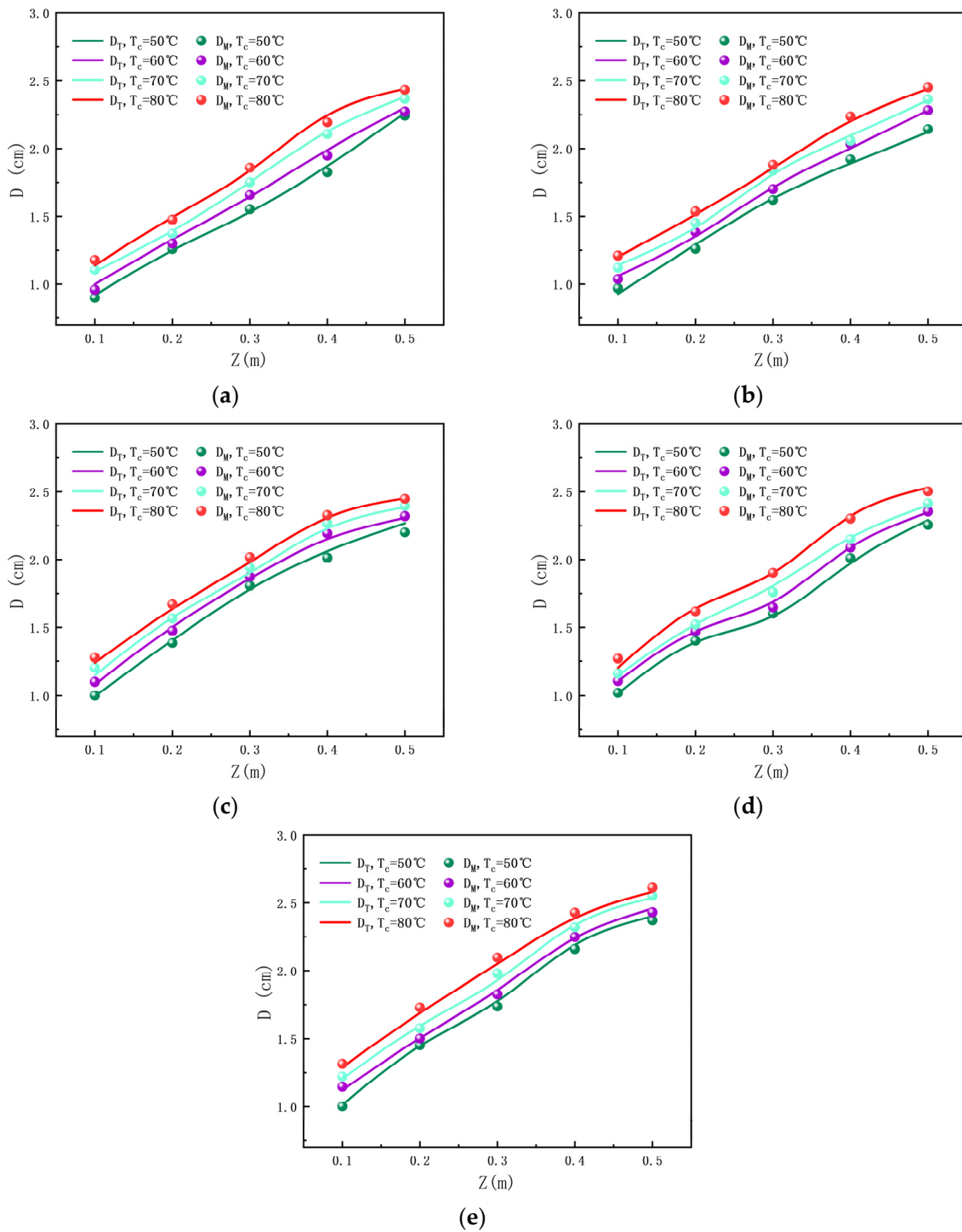


Figure 4. The relationship between bubble diameter and height (Z) under different flow rate ratios. (a): $m_d/m_c = 1:5$. (b): $m_d/m_c = 1:4$. (c): $m_d/m_c = 1:3$. (d): $m_d/m_c = 1:2$. (e): $m_d/m_c = 1:1$.

The bubble growth correlations under different working conditions obtained by different researchers are listed in Table 4. The experimental data are taken into the bubble growth equations in Table 4 to obtain the bubble diameter. Figure 5 shows several bubble growth correlations proposed by previous researchers to compare the correlation and experimental results in this study. Figure 5 shows that, compared to the other correlations,

an improvement of the correlation was necessary. The prediction results of Mahood were consistent with the experimental data in the period of bubble growth beforehand. However, there was a large difference between Mahood’s findings and the experimental data in the period afterward. Figure 5 shows that the bubble growth correlation proposed in this study was the most consistent with the experimental data. This was owing to the bubble growth correlation, which considers the effect of the diameter of the heat exchanger.

Table 4. Bubble growth equations proposed by different researchers.

No	Reference	Correlations	Condition
1	Copper [41]	$R(t) = 2.5 \frac{Ja}{Pr_1^{0.5}} (\alpha t)^{\frac{1}{2}}$	Water, organic liquids, cryogenics and metallic fluids have been used
2	Verhaart et al. [42]	$R(t) = \left\{ \left(\frac{3}{\pi} \right)^{\frac{1}{2}} Ja + \left(\frac{3}{\pi} Ja^2 + 2Ja \right)^{\frac{1}{2}} \right\} D(t)^{\frac{1}{2}}$	All experiments have been carried out at a temperature of 291 K and at (sub)atmospheric pressure(s).
3	Kacamastaf-aogullari [43]	$D_d = 2.64 \times 10^{-5} \left[\frac{\theta}{g(\rho_1 - \rho_v)} \right] \left(\frac{\rho_1 - \rho_v}{\rho_1} \right)^{0.9}$	The average deviation of the correlation is 33%
4	Robinson and Judd [44]	$R(t) = (2Ja\alpha_1 t)^{\frac{1}{2}}$	$36 \leq Ja \leq 63167$
5	Mahood et al. [45]	$D = [D_0^{\frac{3}{2}} - \left(\frac{3k_c}{\rho_v h_{fg}} \right) \left(\frac{k_v}{\pi \epsilon} \right)^{0.5} U_r^{-0.5} \frac{Z^2}{H}]^{\frac{2}{3}}$	Working fluid = water and pentane
6	Brooks et al. [46]	$d_d = 2.11 \times 10^{-3} L_O (Ja_{N,W} N_T)^{-0.49} \rho^*^{-0.78} B_o^{0.44} p_r^{1.72}$ where $B_o = \frac{q_w}{G h_{lv}}$, $Ja_{N,W} = \frac{c_{p,l}(T_w - T_{sat})}{h_{lv}}$, $N_T = \frac{T_w - T_b}{T_w - T_{sat}}$	$Ja_{N,W}: 7.6 \times 10^{-4} - 0.12$; $N_T: 1.0-99$; $\rho^*: 6.4 \times 10^{-4} - 3.4 \times 10^{-2}$; $B_o: 7.3 \times 10^{-5} - 1.0 \times 10^{-3}$;
7	Zhou et al. [47]	$D_s = 0.08 Ja^{0.6} \sqrt{2\theta/g(\rho_1 - \rho_v)}$	
8	Gao et al. [48]	$D_d = \frac{2\sqrt{30}}{15} g t_g^2$	

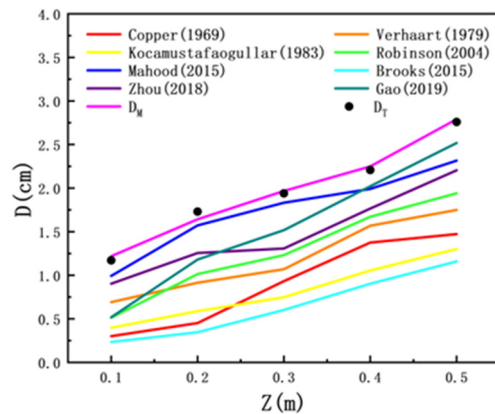


Figure 5. $T_c = 60 \text{ }^\circ\text{C}$, $m_d:m_c = 1:5$, comparison of the bubble growth correlation proposed in this paper with experimental data and other correlations [41–48].

4.2. Local Convective Heat Transfer Coefficient

The calculation of the convective heat transfer coefficient had always been a problem in the DCHE. Previous studies had shown that the Nusselt number represented a criterion number for the intensity of the convective heat transfer coefficient and also represented the ratio of the thermal conductivity of the fluid layer to the convective thermal resistance. At the same time, Vikas Chaurasiya et al. [49] discussed the one-dimensional moving boundary problem and analyzed the influence of size change on heat conduction and convection effects. In addition, many scholars had obtained empirical correlations between the convective heat transfer coefficient of other types of heat exchangers. In this study, an empiric correlation of the local convective heat transfer coefficient between R245fa and Therminol[®]66 in the heat transfer process was derived. According to Equation (18), the local convective heat transfer coefficient of the DCHE was calculated.

As shown in Equation (18), the continuous phase temperature and local convective heat transfer coefficient were closely linked. Figure 6 shows the relationship between the temperature of Therminol[®]66 and local convective heat transfer coefficient. Figure 6 also

shows that the Therminol[®]66 temperature rises while the flow rate ratio and height remain unchanged, and the local convective heat transfer coefficient showed a downward trend with the Therminol[®]66 temperature increase. This was because when the Therminol[®]66 temperature increased, Pr and λ_c decreased, whereas Re increased. However, the increase in Re was smaller than the decrease in Pr and λ_c , which caused the local convective heat transfer coefficient to decrease with increasing temperature. Another reason was that the bubble diameter increases with the increase in continuous phase temperature. This caused thermal resistance (gas phase thermal resistance) to form inside the bubble. The heat transfer between two phases was affected by thermal resistance, which led to the reduction in the local convection heat transfer coefficient [26].

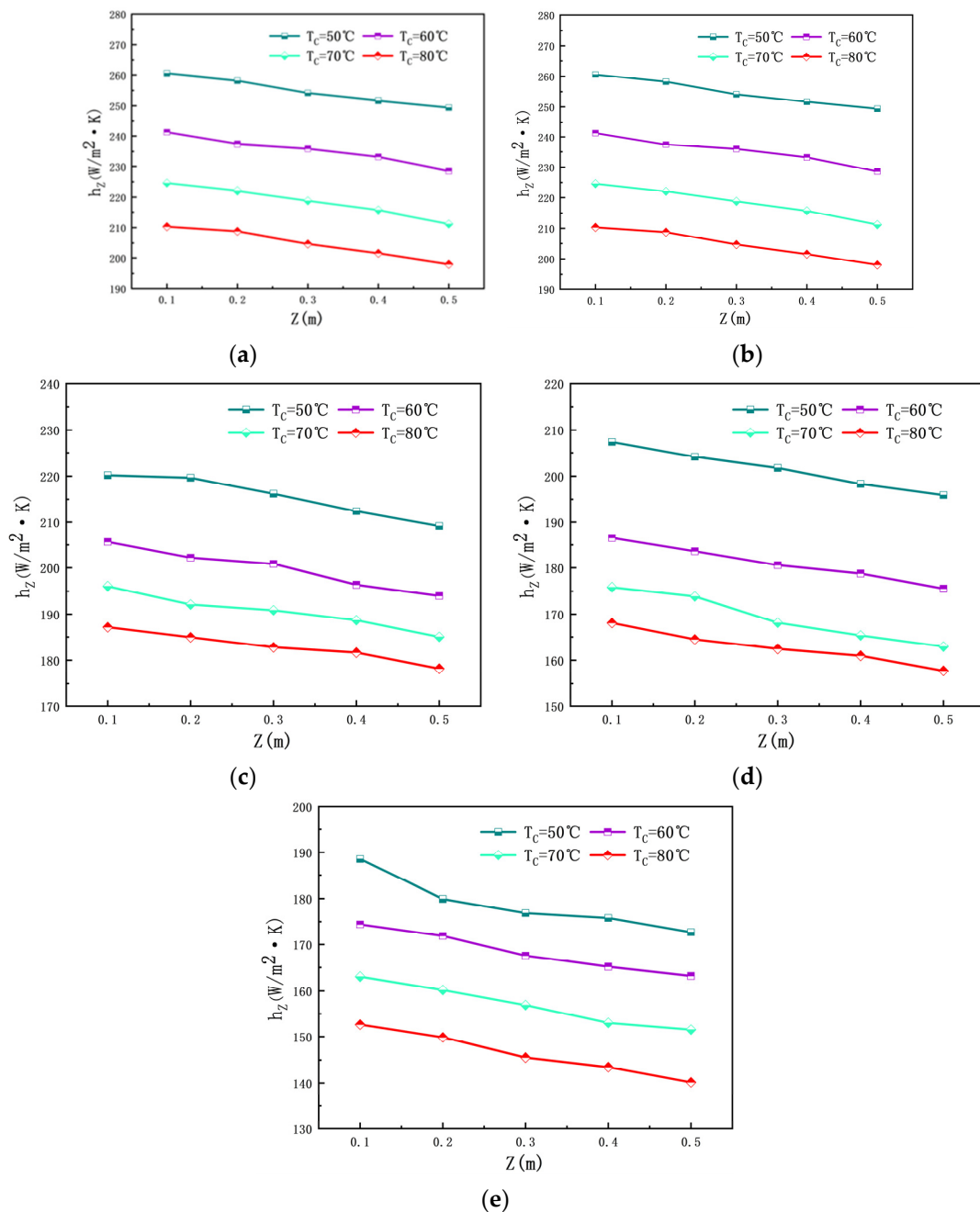


Figure 6. The relationship between the local convective heat transfer coefficient and height (Z) under different flow rate ratios. (a): $m_d/m_c = 1:5$. (b): $m_d/m_c = 1:4$. (c): $m_d/m_c = 1:3$. (d): $m_d/m_c = 1:2$, (e): $m_d/m_c = 1:1$.

Figure 7 shows the connection between the flow rate ratio and local convective heat transfer coefficient. When the other operating conditions were the same, the flow rate ratio was different. The local convective heat transfer coefficient was negatively correlated with the flow rate ratio. When the other working conditions were the same, and the flow rate ratio was 1:5, the local convective heat transfer coefficient was the largest. In the direct contact heat transfer process, when the flow rate ratio decreased, the Therminol[®]66 flow rate increased. As the flow rate of Therminol[®]66 increased, the flow velocity also increased. The increase in continuous phase velocity increased the disturbance in the pipe and destroyed the boundary layer. This led to a local convective heat transfer coefficient increase. At the same time, the low flow rate ratio meant that there was enough energy in the heat exchanger for heat exchange.

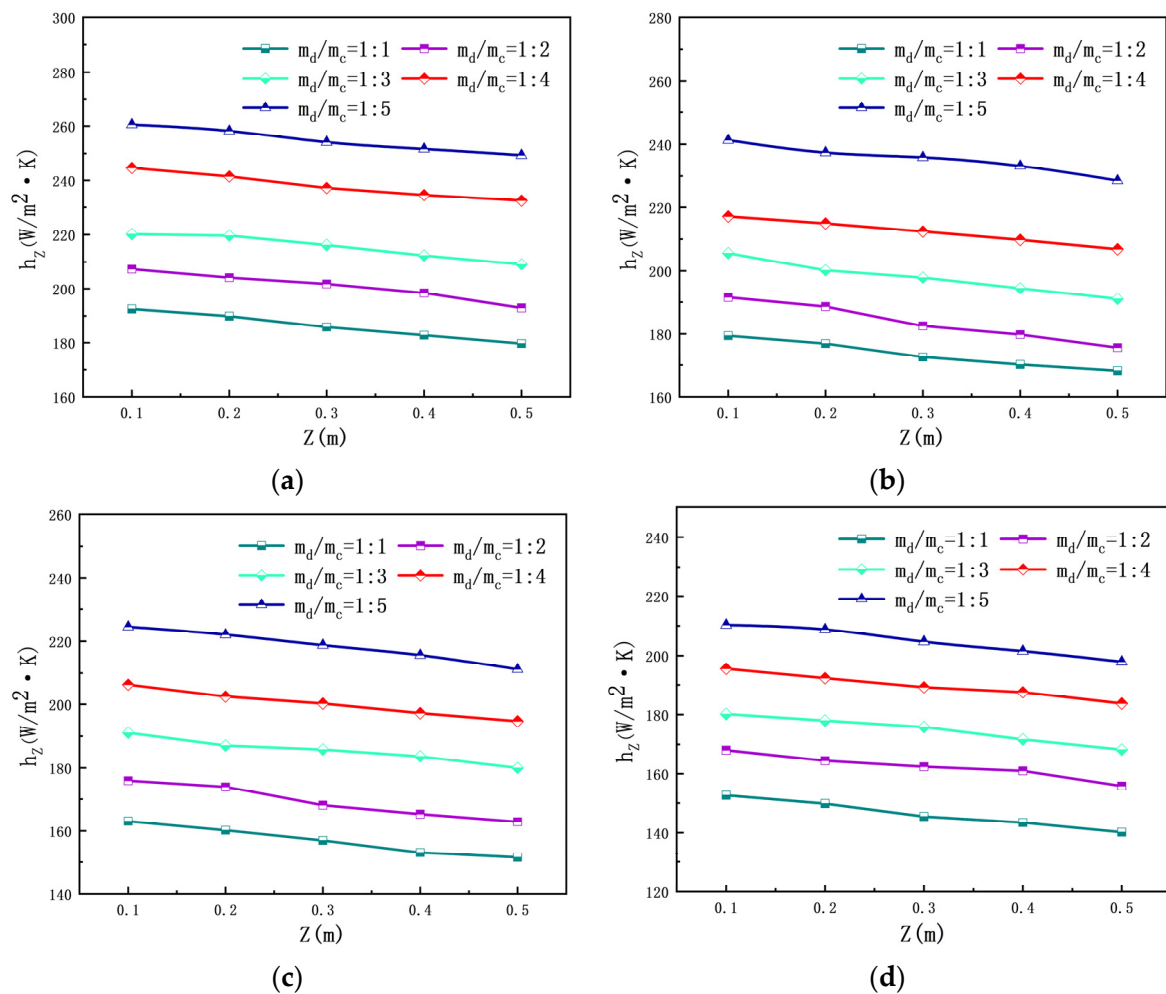


Figure 7. The relationship between the local convective heat transfer coefficient and height (Z) at different temperatures. (a): $T_c = 50$ °C. (b): $T_c = 60$ °C. (c): $T_c = 70$ °C. (d): $T_c = 80$ °C.

The relationship between the local convective heat transfer coefficient and height is shown in Figures 6 and 7, respectively. Figures 6 and 7 show that the local convective heat transfer coefficient decreased as the height increased. This was due to the phase change of the R245fa being at the bottom in the DCHE. The liquid R245fa absorbs the heat of the Therminol[®]66, and the R245fa changes from liquid to vapor. The latent heat of vaporization of the R245fa dominated the direct contact heat transfer process. This led to the phenomenon that the lower the height, the higher the local convective heat transfer coefficient. Another reason was that the temperature difference at the bottom of the DCHE was the largest, which provided more energy for dispersed phase evaporation. The driving

force of temperature difference was the strongest at the bottom of the heat exchanger. Therefore, the heat transfer coefficient was maximum at the bottom.

4.3. Heat Transfer Quantity

The convective heat transfer coefficient indicates the heat transfer capacity among the cold and hot fluids. The Q_Z amount was calculated using the local convective heat transfer coefficient and then compared with Q_T . The accuracy of the local convective heat transfer coefficient was determined.

Figures 8 and 9 show the relationship between the heat transfer quantity and height. As shown in Figures 8 and 9, when the height increased, the heat transfer quantity also grew. When the height was 0.5 m, the heat transfer quantity reached maximum. As shown in Figure 3, when the height increased, the bubble diameter increased, resulting in an increase in the heat exchange area. The heat exchange area was proportional to the heat transfer quantity; therefore, the heat transfer quantity increased with an increase in continuous phase liquid level.

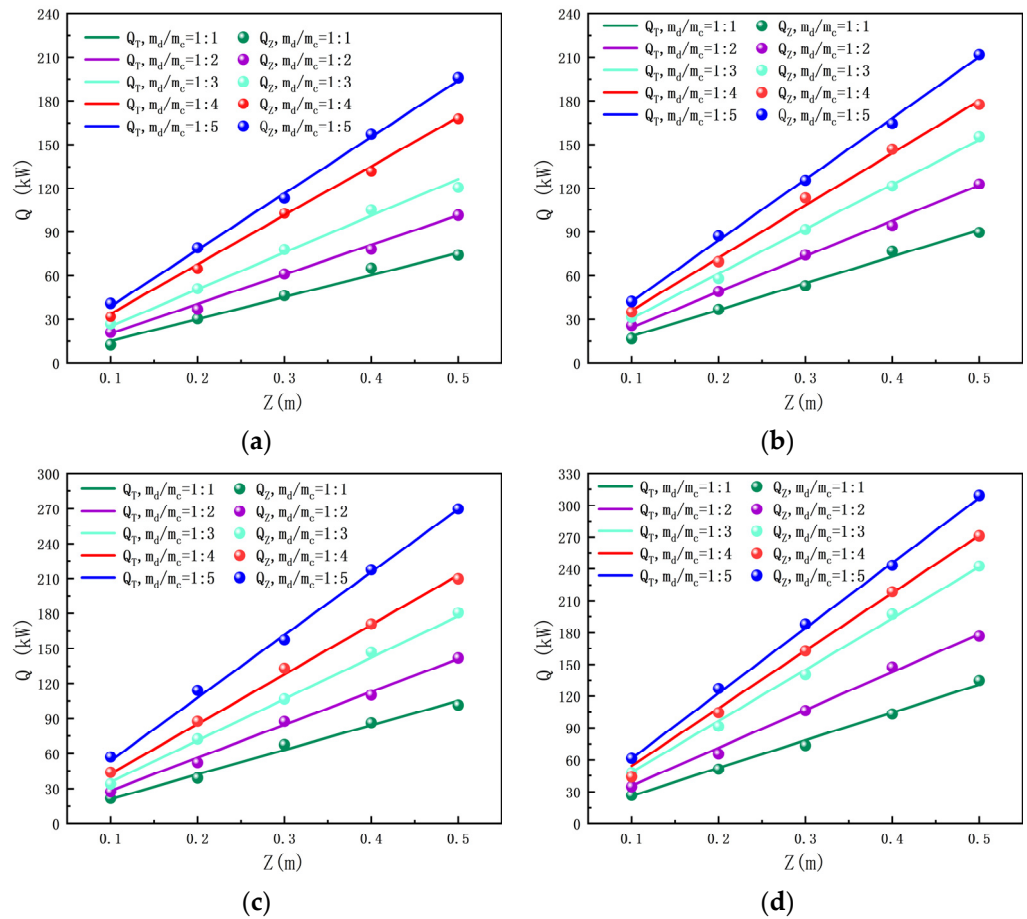


Figure 8. The relationship between heat transfer quantity and height (Z) at different temperatures. (a): $T_c = 50\text{ }^\circ\text{C}$. (b): $T_c = 60\text{ }^\circ\text{C}$. (c): $T_c = 70\text{ }^\circ\text{C}$. (d): $T_c = 80\text{ }^\circ\text{C}$.

Figure 8 shows the relationship between the heat flux and flow rate ratio. Figure 8 shows that the flow rate ratio decreased, and the heat flux increased. When the flow rate ratio was 1:5, the heat flux reached a maximum value. The greater the flow rate of the continuous phase, the greater the heat quantity provided by the Therminol[®]66. Therefore, the heat flux increased as the flow rate of the Therminol[®]66 increased.

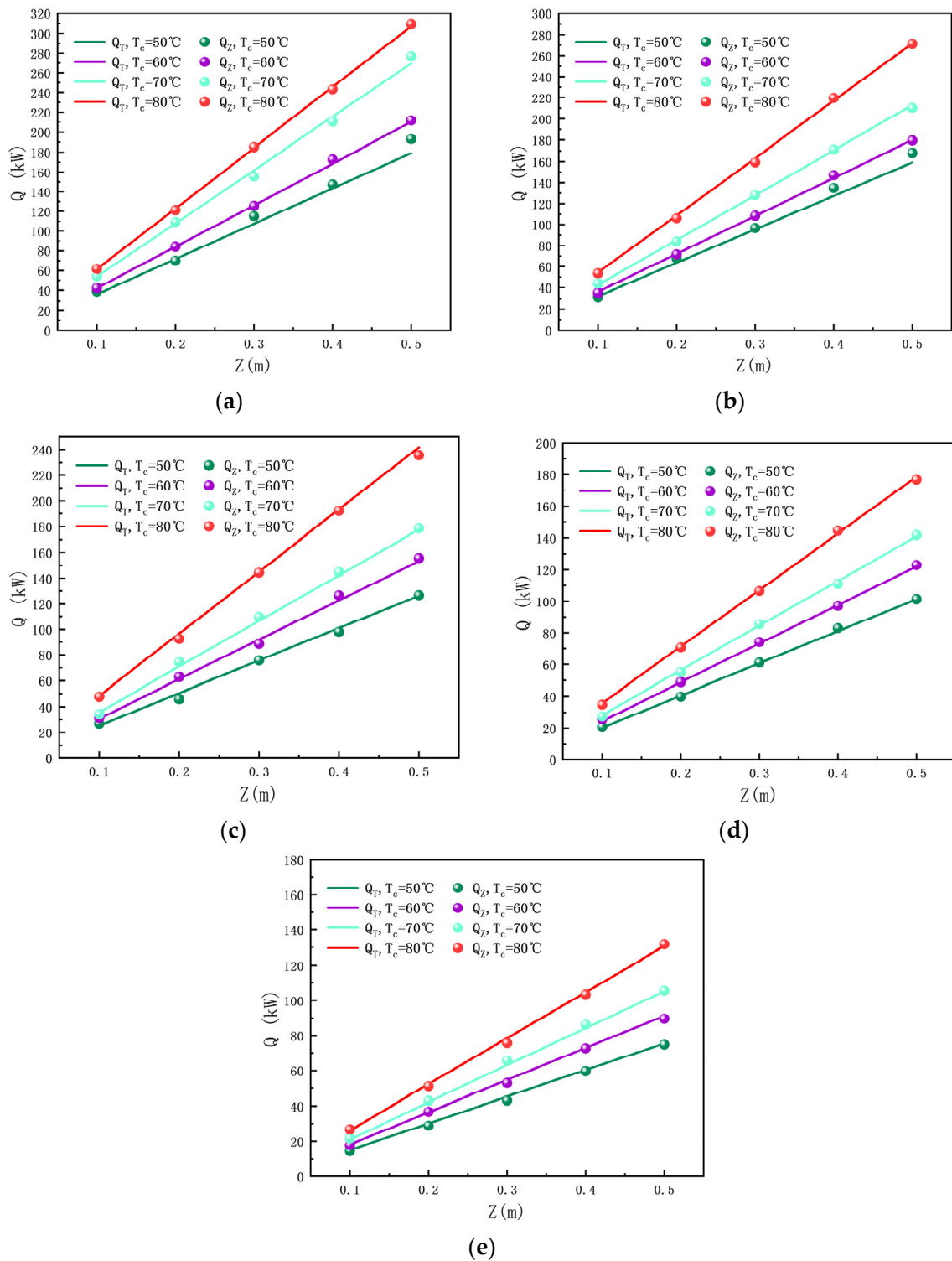


Figure 9. The relationship between heat transfer quantity and height (Z) under different flow rate ratios. (a): $m_d/m_c = 1:5$. (b): $m_d/m_c = 1:4$. (c): $m_d/m_c = 1:3$. (d): $m_d/m_c = 1:2$. (e): $m_d/m_c = 1:1$.

Besides the correlation with height, the relationship between the heat transfer quantity and temperature is shown in Figure 9. As the Therminol[®]66 temperature increased, the heat flux also increased. When the temperature was 80 °C, the heat transfer quantity reached its maximum. This was due to the Therminol[®]66 temperature increase; the heat provided by the Therminol[®]66 also increased. Therefore, the heat flux tended to increase.

The relationship between Q_T and Q_Z is shown in Figures 8 and 9, respectively. The data calculated according to the correlation formula were consistent with the experimental data (Figures 8 and 9). Due to instrumental and measurement uncertainty, the resulting error between the Q_T and Q_Z amounted to 9.4%. (Figure 9a). Within the processing time, the average error between the heat transfer quantity (Q_Z) calculated by the correlation and the actual heat transfer quantity (Q_T) was not more than 10%. The simulated curve satisfactorily reproduced the experimentally observed behavior. However, there was an error between the Q_T and Q_Z . The goal of this paper was to determine the local convective heat transfer coefficient via the simplest method, while guaranteeing a good agreement in the order of magnitude.

Q_Z was calculated using the local convective heat transfer coefficient. It was found that Q_Z and Q_T were in good agreement. Therefore, the local convective heat transfer coefficient calculated using Equation (18) had a high accuracy. The local convective heat transfer coefficient calculated using Equation (18) reduces the calculation workload and solves the problem of calculating the contact area between the dispersed and continuous phases. This lays the foundation for future research on the DCHE.

5. Conclusions

The heat transfer performance of the DCHE was studied experimentally. However, owing to the direct contact heat transfer process, the contact areas of the two phases were difficult to determine. Therefore, the use of the bubble surface area instead of the two-phase contact area was proposed. This paper proposes to accurately evaluate the heat transfer performance of the DCHE by determining the local convective heat transfer coefficient. Based on the experimental conditions, the bubble growth equation for the direct contact heat transfer process under different working conditions was deduced and verified. An empirical correlation formula of the local convective heat transfer coefficient between R245fa and Therminol[®]66 was derived and verified. Therefore, these conclusions were drawn in this study:

1. The bubble diameter was related to the height, Therminol[®]66 temperature, and flow rate ratio. However, the growth of bubbles was significantly affected by the ratio of height and flow rate. At the same time, under different working conditions, the maximum error between the D_M and the D_T was 7%.
2. The local convective heat transfer coefficient was negatively correlated with the height, Therminol[®]66 temperature, and flow rate ratio. When the height was 0.1 m, the continuous phase temperature was 50 °C, the flow rate ratio was 5:1, and the local convective heat transfer coefficient reached the maximum.
3. The heat transfer quantity was positively correlated with the continuous phase temperature, height, and flow rate ratio. Q_Z can be calculated using the empirical correlation formula of the local convective heat transfer coefficient and compared with Q_T . Under different working conditions, the error range of Q_Z and Q_T was within 10%.

Author Contributions: Data curation and writing—original draft preparation, J.Y.; writing—review and editing, B.L.; conceptualization, H.S.; methodology and software, J.X.; investigation, H.W. All authors have read and agreed to the published version of the manuscript.

Funding: This research was funded by the National Natural Science Foundation of China (Project Nos.: 52166004 and U1602272).

Data Availability Statement: Data sharing not applicable.

Conflicts of Interest: The authors declare no conflict of interest.

Nomenclature

Abbreviations

DCHE	direct contact heat exchanger
VHTC	volumetric heat transfer coefficient

Parameters

X_r	uncertainty of the experimental direct measurement data
P_K	precision stint of the apparatus
B_K	error stint
D_M	theoretical bubble diameter, m
D_T	actual bubble diameter, m
h	instantaneous convective heat transfer coefficient of the surface area of the spherical
phase bubble, $W/m^2 \cdot ^\circ C$	
ΔT	temperature difference between the R245fa and Therminol [®] 66, K
ρ_{dv}	vapor phase density of the dispersed phase, kg/m
h_{fg}	latent heat of condensation, kJ/kg
ΔT_{min}	minimum temperature difference, K
ΔT_{max}	maximum temperature difference, K
H	continuous phase liquid level, m
Z	position of bubble, m
T_c	temperatures of continuous phase, K
T_d	temperatures of dispersed phase, K
$T_{c,out}$	outlet temperatures of continuous phase, K
$T_{c,in}$	inlet temperatures of continuous phase, K
$T_{d,out}$	outlet temperatures of dispersed d phase, K
$T_{d,in}$	inlet temperatures of dispersed phase, K
Nu	Nusselt number
Pe	Peclet number
λ_c	thermal conductivity of continuous phase, $W/(m \cdot K)$
t_v	time required for complete evaporation, s
U_r	relative speed of the R245fa and Therminol [®] 66, m/s
ϵ_d	thermal diffusivity of the R245fa, m^2/s
U	rising speed of the bubble, m/s
w	ratio of relative velocity to bubble velocity
D_0	nozzle diameter, m
h_Z	local convective heat transfer coefficient, $W/m^2 \cdot K$
n	number of local two-phase bubbles
Q_T	actual heat transfer quantity, kW
Q_Z	theoretical heat transfer quantity, kW
m_d	mass flow rate of the dispersed phase, kg/h
$H_{d,out}$	outlet enthalpy of the dispersed phase, kJ/kg
$H_{d,in}$	inlet enthalpy of the dispersed phase, kJ/kg
A	two-phase contact area, m^2
i	variable
r_i	theoretical radius of the i-th bubble, m
$D_{i,M}$	theoretical diameter of the i-th bubble, m
ΔT_{tm}	logarithmic average temperature difference between the R245fa and Therminol [®] 66, K

References

1. Cui, Z.; Du, Q.; Gao, J.; Bie, R.; Li, D. Development of a direct contact heat exchanger for energy and water recovery from humid flue gas. *Appl. Therm. Eng.* **2020**, *173*, 115214. [[CrossRef](#)]
2. Maalouf, S.; Boulawz Ksayer, E.; Clodic, D. Investigation of direct contact condensation for wet flue-gas waste heat recovery using Organic Rankine Cycle. *Energy Convers. Manag.* **2016**, *107*, 96–102. [[CrossRef](#)]
3. Kim, T.Y.; Negash, A.; Cho, G. Experimental and numerical study of waste heat recovery characteristics of direct contact thermoelectric generator. *Energy Convers. Manag.* **2017**, *140*, 273–280. [[CrossRef](#)]

4. Brückner, S.; Liu, S.; Miró, L.; Radspieler, M.; Cabeza, L.F.; Lävemann, E. Industrial waste heat recovery technologies: An economic analysis of heat transformation technologies. *Appl. Energy* **2015**, *151*, 157–167. [[CrossRef](#)]
5. Yabuki, T.; Nakabeppu, O. Microscale wall heat transfer and bubble growth in single bubble subcooled boiling of water. *Int. J. Heat Mass Transf.* **2016**, *100*, 851–860. [[CrossRef](#)]
6. Edel, Z.J.; Mukherjee, A. Experimental investigation of vapor bubble growth during flow boiling in a microchannel. *Int. J. Multiph. Flow* **2011**, *37*, 1257–1265. [[CrossRef](#)]
7. Cai, C.; Liu, H.; Xi, X.; Jia, M.; Yin, H. Bubble growth model in uniformly superheated binary liquid mixture. *Int. J. Heat Mass Transf.* **2018**, *127*, 629–638. [[CrossRef](#)]
8. Thiagarajan, S.J.; Yang, R.; King, C.; Narumanchi, S. Bubble dynamics and nucleate pool boiling heat transfer on microporous copper surfaces. *Int. J. Heat Mass Transf.* **2015**, *89*, 1297–1315. [[CrossRef](#)]
9. Ghazivini, M.; Hafez, M.; Ratanpara, A.; Kim, M. A review on correlations of bubble growth mechanisms and bubble dynamics parameters in nucleate boiling. *J. Therm. Anal. Calorim.* **2022**, *147*, 6035–6071. [[CrossRef](#)]
10. Mao, L.; Zhou, W.; Hu, X.; He, Y.; Zhang, G.; Zhang, L.; Fu, R. Pool boiling performance and bubble dynamics on graphene oxide nanocoating surface. *Int. J. Therm. Sci.* **2020**, *147*, 106154. [[CrossRef](#)]
11. Xu, J.; Xiao, Q.; Chen, Y.; Fei, Y.; Pan, J.; Wang, H. A modified L2-star discrepancy method for measuring mixing uniformity in a direct contact heat exchanger. *Int. J. Heat Mass Transf.* **2016**, *97*, 70–76. [[CrossRef](#)]
12. Xu, J.; Xiao, Q.; Lv, Z.; Huang, J.; Xiao, R.; Pan, J.; Wang, H. New metrics for measuring multiphase mixing effects in a direct-contact heat exchanger. *Appl. Therm. Eng.* **2019**, *147*, 592–601. [[CrossRef](#)]
13. Xiao, Q.; Pan, J.; Lv, Z.; Xu, J.; Wang, H. Measure of bubble non-uniformity within circular region in a direct-contact heat exchanger. *Int. J. Heat Mass Transf.* **2017**, *110*, 257–261. [[CrossRef](#)]
14. Fei, Y.; Xiao, Q.; Xu, J.; Pan, J.; Wang, S.; Wang, H.; Huang, J. A novel approach for measuring bubbles uniformity and mixing efficiency in a direct contact heat exchanger. *Energy* **2015**, *93*, 2313–2320. [[CrossRef](#)]
15. Xiao, Q.; Yang, K.; Wu, M.; Pan, J.; Xu, J.; Wang, H. Complexity evolution quantification of bubble pattern in a gas-liquid mixing system for direct-contact heat transfer. *Appl. Therm. Eng.* **2018**, *138*, 832–839. [[CrossRef](#)]
16. Sun, H.; Li, Z.; Wang, S.; Xu, J.; Wang, H. Evolution and quantification of distribution uniformity of bubbles using computational geometry. *Chem. Eng. Sci.* **2022**, *247*, 116910. [[CrossRef](#)]
17. Wen, X.; Liang, C.; Zhang, X. Experimental study on heat transfer coefficient between air and liquid in the cross-flow heat-source tower. *Build. Environ.* **2012**, *57*, 205–213. [[CrossRef](#)]
18. Kunkel, S.; Teumer, T.; Dörnhöfer, P.; Wunder, F.; Repke, J.; Rädle, M. Investigation of heat transfer coefficients in a liquid-liquid direct contact latent heat storage system. *J. Energy Storage* **2020**, *28*, 101178. [[CrossRef](#)]
19. Mahood, H.B.; Campbell, A.N.; Thorpe, R.B.; Sharif, A.O. Heat transfer efficiency and capital cost evaluation of a three-phase direct contact heat exchanger for the utilisation of low-grade energy sources. *Energy Convers. Manag.* **2015**, *106*, 101–109. [[CrossRef](#)]
20. Mahood, H.B.; Sharif, A.O.; Al-Aibi, S.; Hawkins, D.; Thorpe, R. Analytical solution and experimental measurements for temperature distribution prediction of three-phase direct-contact condenser. *Energy* **2014**, *67*, 538–547. [[CrossRef](#)]
21. Mahood, H.B.; Campbell, A.N.; Sharif, A.O.; Thorpe, R.B. Heat transfer measurement in a three-phase direct-contact condenser under flooding conditions. *Appl. Therm. Eng.* **2016**, *95*, 106–114. [[CrossRef](#)]
22. Nomura, T.; Tsubota, M.; Oya, T.; Okinaka, N.; Akiyama, T. Heat release performance of direct-contact heat exchanger with erythritol as phase change material. *Appl. Therm. Eng.* **2013**, *61*, 28–35. [[CrossRef](#)]
23. Nomura, T.; Tsubota, M.; Sagara, A.; Okinaka, N.; Akiyama, T. Performance analysis of heat storage of direct-contact heat exchanger with phase-change material. *Appl. Therm. Eng.* **2013**, *58*, 108–113. [[CrossRef](#)]
24. Nomura, T.; Tsubota, M.; Oya, T.; Okinaka, N.; Akiyama, T. Heat storage in direct-contact heat exchanger with phase change material. *Appl. Therm. Eng.* **2013**, *50*, 26–34. [[CrossRef](#)]
25. Barabash, P.; Solomakha, A.; Sereda, V. Experimental investigation of heat and mass transfer characteristics in direct contact exchanger. *Int. J. Heat Mass Transf.* **2020**, *162*, 120359. [[CrossRef](#)]
26. Wang, Y.; Fu, H.; Huang, Q.; Cui, Y.; Sun, Y.; Jiang, L. Experimental study of direct contact vaporization heat transfer on n-pentane-water flowing interface. *Energy* **2015**, *93*, 854–863. [[CrossRef](#)]
27. Fu, H.; Ma, L.; Wang, H. Direct-Contact Heat Transfer during n-Pentane Vaporization in a Two-Dimensional Water Column. *Chem. Eng. Technol.* **2020**, *43*, 1416–1423. [[CrossRef](#)]
28. Fu, H.; Wang, Y.; Huang, Q.; Cui, Y.; Sun, Y.; Jiang, L. Direct contact evaporation heat transfer coefficient and drobble size distribution in a 2D column. *Appl. Therm. Eng.* **2016**, *96*, 568–575. [[CrossRef](#)]
29. Kim, J.H.; Simon, T.W.; Viskanta, R. Journal of heat transfer policy on reporting uncertainties in experimental measurements and results. *J. Heat Transf.* **1993**, *115*, 5–6. [[CrossRef](#)]
30. Moffat, R.J. Describing the uncertainties in experimental results. *Exp. Therm. Fluid Sci.* **1988**, *1*, 3–17. [[CrossRef](#)]
31. Mori, Y.H. An analytic model of direct-contact heat transfer in spray-column evaporators. *AIChE J.* **1991**, *37*, 539–546. [[CrossRef](#)]
32. Moalem-Maron, D.; Sokolov, M.; Sideman, S. A closed periodic condensation-evaporation cycle of an immiscible, gravity driven bubble. *Int. J. Heat Mass Transf.* **1980**, *23*, 1417–1424. [[CrossRef](#)]
33. Shimizu, Y.; Mori, Y.H. Evaporation of single liquid drops in an immiscible liquid at elevated pressures: Experimental study with n-pentane and R 113 drops in water. *Int. J. Heat Mass Transf.* **1988**, *31*, 1843–1851. [[CrossRef](#)]

34. Chaurasiya, V.C.R.K. A numerical study of a moving boundary problem with variable thermal conductivity and temperature-dependent moving PCM under periodic boundary condition. *Eur. Phys. J. Plus* **2022**, *137*, 714. [[CrossRef](#)]
35. Prasser, H.M.; Beyer, M.; Böttger, A.; Carl, H.; Lucas, D.; Schaffrath, A.; Schütz, P.; Weiss, F.P.; Zschau, J. Influence of the Pipe Diameter on the Structure of the Gas-Liquid Interface in a Vertical Two-Phase Pipe Flow. *Nucl. Technol.* **2005**, *152*, 3–22. [[CrossRef](#)]
36. Vafaei, S.T.B.A. Theoretical and experimental investigation of quasi-steady-state bubble growth on top of submerged stainless steel nozzles. *Colloids Surf. A Physicochem. Eng. Asp.* **2010**, *369*, 11–19. [[CrossRef](#)]
37. Baqir, A.S.; Mahood, H.B.; Campbell, A.N.; Griffiths, A.J. Measuring the average volumetric heat transfer coefficient of a liquid–liquid–vapour direct contact heat exchanger. *Appl. Therm. Eng.* **2016**, *103*, 47–55. [[CrossRef](#)]
38. Liu, Q.; Zhang, Y.; Wu, Y.; Lyu, J.; Liu, Q. Bubble Growth in NaCl Solution: Influence of Superheat Temperature and Solution Concentration. *Ind. Eng. Chem. Res.* **2021**, *60*, 4440–4452. [[CrossRef](#)]
39. Xu, J.H.; Luo, G.S.; Li, S.W.; Chen, G.G. Shear force induced monodisperse droplet formation in a microfluidic device by controlling wetting properties. *Lab A Chip* **2006**, *6*, 131–136. [[CrossRef](#)]
40. Djeridi, H.; Gabillet, C.; Billard, J.Y. Two-phase Couette–Taylor flow: Arrangement of the dispersed phase and effects on the flow structures. *Phys. Fluids* **2004**, *16*, 128–139. [[CrossRef](#)]
41. Cooper, M.G. The microlayer and bubble growth in nucleate pool boiling. *Int. J. Heat Mass Transf.* **1969**, *12*, 915–933. [[CrossRef](#)]
42. Verhaart, H.F.A.R. Growth rate of a gas bubble during electrolysis in supersaturated liquid. *Int. J. Heat Mass Transf.* **1980**, *23*, 293–299. [[CrossRef](#)]
43. Kocamustafaogullari, G. Pressure dependence of bubble departure diameter for water. *Int. Commun. Heat Mass Transf.* **1983**, *10*, 501–509. [[CrossRef](#)]
44. Robinson, A.J.; Judd, R.L. The dynamics of spherical bubble growth. *Int. J. Heat Mass Transf.* **2004**, *47*, 5101–5113. [[CrossRef](#)]
45. Mahood, H.B.; Campbell, A.N.; Thorpe, R.B.; Sharif, A.O. Experimental measurements and theoretical prediction for the volumetric heat transfer coefficient of a three-phase direct contact condenser. *Int. Commun. Heat Mass Transf.* **2015**, *66*, 180–188. [[CrossRef](#)]
46. Brooks, C.S.; Hibiki, T. Wall nucleation modeling in subcooled boiling flow. *Int. J. Heat Mass Transf.* **2015**, *86*, 183–196. [[CrossRef](#)]
47. Zhou, J.; Zhang, Y.; Wei, J. A modified bubble dynamics model for predicting bubble departure diameter on micro-pin-finned surfaces under microgravity. *Appl. Therm. Eng.* **2018**, *132*, 450–462. [[CrossRef](#)]
48. Gao, W.; Qi, J.; Yang, X.; Zhang, J.; Wu, D. Experimental investigation on bubble departure diameter in pool boiling under sub-atmospheric pressure. *Int. J. Heat Mass Transf.* **2019**, *134*, 933–947. [[CrossRef](#)]
49. Chaurasiya, V.; Wakif, A.; Shah, N.A.; Singh, J. A study on cylindrical moving boundary problem with variable thermal conductivity and convection under the most realistic boundary conditions. *Int. Commun. Heat Mass Transf.* **2022**, *138*, 106312. [[CrossRef](#)]

Disclaimer/Publisher’s Note: The statements, opinions and data contained in all publications are solely those of the individual author(s) and contributor(s) and not of MDPI and/or the editor(s). MDPI and/or the editor(s) disclaim responsibility for any injury to people or property resulting from any ideas, methods, instructions or products referred to in the content.